Comparison of three isoelectronic multiple-well reaction systems: OH + CH2O, OH + CH2CH2, and OH + CH2NH

ARTICLE *in* THE JOURNAL OF PHYSICAL CHEMISTRY A · APRIL 2015

Impact Factor: 2.69 · DOI: 10.1021/acs.jpca.5b00910 · Source: PubMed

2 AUTHORS, INCLUDING:

Akbar Ali Moahamad

University of Michigan

12 PUBLICATIONS **53** CITATIONS

THE JOURNAL OF PHYSICAL CHEMISTRY A

Article

pubs.acs.org/JPCA

Comparison of Three Isoelectronic Multiple-Well Reaction Systems: OH + CH_2O, OH + CH_2CH_2, and OH + CH_2NH

Mohamad Akbar Ali and John R. Barker*

Department of Atmospheric, Ocean, and Space Sciences, The University of Michigan, Ann Arbor, Michigan 48109-2143, United States

Supporting Information

ABSTRACT: Methylenimine (CH_2NH) has been predicted to be a product of the atmospheric photo-oxidation of methylamine, but its atmospheric reactions have not been measured. In this paper, we report potential energy surfaces (PESs) and rate constants for OH + CH_2NH and its isoelectronic analogues OH + CH_2O and OH + CH_2CH_2, which are more fully understood. The PESs were computed using the BHandHLYP/aug-cc-pVTZ and CCSD(T)/aug-cc-pVTZ levels of theory. Canonical variational transition state theory and Rice−Ramsperger−Kassel−Marcus and master equation modeling were used to calculate temperature- and pressure-dependent rate constants, with particular emphasis on the OH + reactant entrance channels and the effects of prereactive complexes. The computed results are in reasonable agreement with experimental data where they can be compared and also with the results of previous theoretical calculations. The results show that to some extent OH radicals both add to the carbon center double bond in CH_2NH and abstract methylene hydrogen atoms, as in the OH + CH_2O and OH + CH_2CH_2 reactions, respectively, but the dominant pathway is abstraction of the hydrogen from N−H. The computed rate constants are suitable for both atmospheric and combustion modeling.

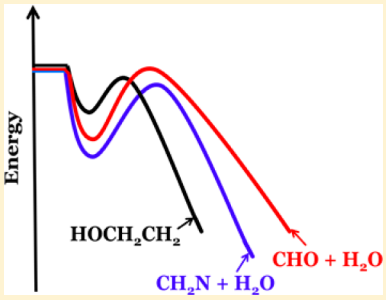

1. INTRODUCTION

The alkyl amines, especially methylamine (CH_3NH_2), dimethylamine [$(CH_3)_2NH$], and trimethylamine [$(CH_3)_3N$], are emitted to the atmosphere from a wide range of sources, including animal husbandry, food processing, marine emissions, biomass burning, and carbon capture storage (CCS) technologies.[1,2] Ethylamine has been used as a model compound for biomass combustion of amino compounds. These amines are also potential atmospheric precursors of HCN and N_2O. The latter is a greenhouse gas and the main source of stratospheric NOx.[3,4]

Once emitted to the atmosphere, amines are expected to react with ambient OH radicals. The expected products are mainly carbon-centered amino radicals, with lesser yields of nitrogen-centered imino radicals. For example, aminomethyl radical ($\bullet CH_2NH_2$) is the dominant product and methylimine radical [$CH_3N(\bullet)H$] is a minor product of the reaction of OH with methylamine.[1,2] The major products from the photo-oxidation of methylamine are nitrosamine, a carcinogen, and methylenimine (CH_2NH); other amines yield analogous imines.[2,5] CH_2NH also can be produced by pyrolysis of amines and azides.[6] In particular, methyl azide decomposes to produce CH_2NH, hydrogen cyanide (HCN), and hydrogen isocyanide (HNC), which are important not only in conventional atmospheric chemistry and combustion but also in astrophysical environments. The CH_2NH molecule has been characterized spectroscopically,[7−11] which has enabled its detection in the interstellar medium and in ices on the comet C/1995 O1 (Hale−Bopp). Its presence has been suggested in the icy surfaces of Pluto and Triton (Neptune's largest moon) and in Titan's upper atmosphere.[6,12−14] In astrobiology, these N-containing molecules are thought to have a significant role in the synthesis of prebiotic molecules. For example, it has been suggested that CH_2NH might react either with HCN or HNC in interstellar ice particles to produce aminoacetonitrile, a precursor of glycine.[15,16]

The atmospheric fate of CH_2NH is not known with certainty because no direct measurements of its reaction kinetics have been carried out. The compound is highly reactive, soluble in water, and sticky, thus posing severe experimental challenges.[2] In the absence of experiments, theoretical methods offer the best alternative approach to investigate the reactions of CH_2NH. While the present paper was in preparation, Bunkan et al.[17] reported rate constants for the OH + CH_2NH reaction system calculated using Rice−Ramsperger−Kassel−Marcus (RRKM) theory on the basis of energies and vibrational parameters computed at the CCSD(T)/cc-PV(TQ)Z//CCSD-(T)/cc-pVTZ level of theory (designated CC-pQ//CC-p). They used the long-range transition state theory method of Georgievskii and Klippenstein[18] to estimate the capture rate constant [$k(T) = 4.86 \times 10^{-10}(T/298\ \mathrm{K})^{-1/6}$ cm^3 molecule^{-1} s^{-1}], which they employed with the inverse Laplace transform method and the master equation (ME) code MESMER[19] to predict temperature- and pressure-dependent rate constants for the

Special Issue: 100 Years of Combustion Kinetics at Argonne: A Festschrift for Lawrence B. Harding, Joe V. Michael, and Albert F. Wagner

Received: January 28, 2015
Revised: April 1, 2015
Published: April 3, 2015

DOI: 10.1021/acs.jpca.5b00910
J. Phys. Chem. A 2015, 119, 7578−7592

reaction system. In the present work, we have also used RRKM theory and an ME code, MultiWell,[20−22] to compute rate constants at a similar level of theory. Instead of using the generic approximations found in long-range transition state theory, we have used variational transition state theory (VTST) to compute the capture rate constants with parameters based on constrained optimizations along the reaction path. In order to assess the accuracy of our methods, we have also carried out calculations on the OH + CH_2O and OH + C_2H_4 systems, which are isoelectronic with OH + CH_2NH. The comparison of the three systems computed at the same level of theory provides more confidence in the results. We have carried out calculations for temperatures and pressures suitable for both atmospheric and combustion modeling.

Many experimental and theoretical studies of the OH + CH_2O reaction system have been performed,[23−28] and it is known that hydrogen abstraction is the only important channel from 200 to 400 K. Recent high-temperature and high-pressure experimental rate constants measured by Wang et al.[26] exhibit a positive temperature dependence (i.e., the rate constant increases with temperature). The experimental data have been critically reviewed.[29−31] In recent theoretical studies, Zhang et al.[28] located stationary points on the OH + CH_2O PES at the CCSD(T)//MP2(Full) + ZPE × 0.95 with 6-311+G(df,pd) basis set.[28] Their computed rate constant at 298 K is ∼4 times larger than the recommended value,[29−31] which is based on experimental measurements.[23−25] In a previous study, Xu et al.[27] computed the rate constants for both abstraction and addition at the CCSD(T)/6-311+G(3df,2p)//CCSD/6-311++G(d,p) and CCSD(T)/6-311+G(3df,2p)// B3LYP/6-311++G(3df,2p) levels of theory.[27] The temperature-dependent rate constant in their study is ∼2 times larger than the experimental value at 298 K.[23−25]

Theoretical and experimental studies on OH + C_2H_4 have been carried out by several research groups.[32−40] Theoretical studies by Golden,[36] Greenwald et al.,[37] Senosiain et al.,[38] Cleary et al.,[39] and Zhu et al.[40] employed different quantum-chemical and kinetics methods to model OH + CH_2CH_2, but the results are in reasonable agreement. With minor adjustments of reaction barrier heights, the theoretical results are also in good agreement with experiments. The results show that the OH radical essentially exclusively adds to the sp^2 carbon atom under atmospheric conditions, but hydrogen abstraction becomes important in combustion systems at temperatures above 800 K,[33,38] as shown by laser-induced fluorescence experiments[33] and a theoretical study.[38]

The OH + CH_2O and OH + CH_2CH_2 reactions are important in both the atmosphere and in combustion. The fate of CH_2NH in either environment is not known with certainty. The goal of the present study is to compute temperature- and pressure-dependent rate constants for the OH + CH_2NH reaction and compare them with their counterparts in the other isoelectronic reactions. The current study provides detailed reaction mechanisms for all three isoelectronic reaction systems. A central focus is on transition-state optimizations, barrier heights, and computed rate constants for the association channels. The effects of prereactive complexes, which are ubiquitous in reactions involving OH radicals, are analyzed in considerable detail.

In the following sections, we first describe the theoretical methods used for electronic structure and kinetics and then discuss the results obtained for each reaction system. Experimental and theoretical enthalpies of reaction and reaction rate constants are compared in order to assess the accuracy of the theoretical methods. Finally, conclusions and recommendations are presented.

2. METHODS

2.1. Electronic Structure. Most of the ab initio calculations and all of the density functional theory (DFT) calculations were carried out using the Gaussian 09 suite of programs.[41] Geometries of all stationary points on each PES were optimized using the BHandHLYP/aug-cc-pVTZ level of theory[42−44] (designated BH-a), which was also used to obtain the vibrational parameters. The results are tabulated in the Supporting Information. Some calculations were also carried out at the B3LYP/aug-cc-pVTZ level of theory.[45] Single-point energy calculations were carried out at the CCSD(T)/aug-cc-pVTZ (designated CC-a) level of theory[43,44,46] using the BH-a-optimized geometries (designated CC-a//BH-a). This combination of BHandHLYP with CCSD(T) with the Dunning-type basis set has been tested by other groups[47−49] and shown to be reasonably accurate. For some important species in the OH + CH_2O and OH + CH_2NH reactions, both the geometry optimizations and the vibrational analysis were carried out at the CCSD(T)/aug-cc-pVTZ//CCSD(T)/aug-cc-pVTZ level of theory (designated CC-a//CC-a) using the CFOUR suite of programs.[50]

The CC-a/BH-a level of theory typically gives results that are accurate to ∼2 kcal/mol, and CC-a//CC-a level is typically accurate to about ∼1 kcal/mol.[51] Rate constants obtained previously by our group for CH_4 + Cl using the CC-a//CC-a level of theory were in very good agreement with experimental data.[52] Previous theoretical studies of other reactions have also obtained accurate rate constants using CCSD(T) with Dunning basis sets,[52−54] The two levels of theory produced similar optimized geometries of reactants, complexes, and products, but the geometries and vibrational frequencies of the transition states differed significantly.

For open- and closed-shell species, reference wave functions were based on unrestricted Hartree−Fock (UHF) and restricted Hartree−Fock (RHF), respectively. Intrinsic reaction coordinate (IRC) calculations[55,56] were carried out to confirm the identities of the reactants and products for every transition state. The T1 diagnostic (computed using CC-a//BH-a) for each important species was ≤0.04, a recommended maximum acceptable for a single-reference wave function as suggested by Rienstra-Kiracofe et al.[57] The spin expectation value $\langle S^2 \rangle$ for each species calculated at the BH-a level of theory was ∼0.75, indicating that spin contamination was negligible. The "GUESS=MIX" keyword was used for the transition states of addition reactions. The "GUESS=MIX" option mixes the HOMO and LUMO orbitals to break spatial symmetry, resulting in a better description of the wave function for these transition states.

2.2. Kinetics. All of the kinetics calculations were carried out using programs in the MultiWell program suite.[20−22] The high-pressure-limit rate constants were calculated using canonical TST with Eckart asymmetric tunneling corrections. The unimolecular rate constant in the high-pressure limit, $k_\infty^{\mathrm{uni}}(T)$, which is the same as the canonical TST rate constant $k^{\mathrm{CTST}}(T)$, is given by eq 1:[58]

$$k^{\mathrm{CTST}}(T) = k_\infty^{\mathrm{uni}}(T) = \Gamma L^{\ddagger} \times \frac{k_B T}{h} \frac{Q_{TS}^{\ddagger}}{Q_R} \exp\left(-\frac{\Delta E_0^{\ddagger}}{k_B T}\right) \quad (1)$$

DOI: 10.1021/acs.jpca.5b00910
J. Phys. Chem. A 2015, 119, 7578−7592

where Γ is the quantum-mechanical tunneling correction, h is Planck's constant, k_B is Boltzmann's constant, $\Delta E_0^{\ddagger}$ is the zero-point energy (ZPE)-corrected energy difference between the transition state and the reactants, $Q_{TS}^{\ddagger}$ and Q_R are the total partition functions for the transition state and the reactants, respectively, and $L^{\ddagger}$ is the reaction path degeneracy, given by

$$L^{\ddagger} = \frac{m^{\ddagger}}{m} \times \frac{\sigma_{ext}}{\sigma_{ext}^{\ddagger}}$$

in which $m^{\ddagger}$ and m are the numbers of optical isomers of the transition state and reactant, respectively, and $\sigma_{ext}^{\ddagger}$ and σ_{ext} are the external rotation symmetry numbers of the transition state and reactant, respectively. The partition functions were computed using the ro-vibrational parameters obtained from the quantum-chemical calculations. We used unscaled vibrational frequencies in our calculations. The electronic partition function for the two lowest electronic states of the OH radical ($^2\Pi_{3/2}$ and $^2\Pi_{1/2}$) was included with the 139.7 cm^{-1} splitting due to spin−orbit coupling: $Q_{OH}^{elec} = 2 + 2\exp(-139.7\ cm^{-1}/k_B T)$.[59] The spin−orbit coupling of the prereactive complexes and transition states were assumed to be negligible.[17,38,54] The recombination rate constant and corresponding unimolecular dissociation rate constant are related as $k_{\infty}^{rec} = K_{eq} k_{\infty}^{uni}$, where K_{eq} is the equilibrium constant.

The lower-frequency normal mode vibrations in some of the transition states can be approximately described as large-amplitude torsions, which were identified by visualizing them with GaussView.[60] These were treated as one-dimensional (1-D) unsymmetrical hindered internal rotations with hindrance potentials and mass factors obtained using the BH-a level of theory. For unsymmetrical internal rotors, the 1-D torsional potentials were computed by carrying out constrained geometry optimizations at fixed dihedral angles ("relaxed scans") and are reported in the Supporting Information; the angle-dependent mass factor was assumed to be a constant (based on the minimum-energy structure) in this work. As explained in the MultiWell User Manual, the torsional potential needed to compute the eigenstates for unsymmetrical hindered rotors was fitted to a Fourier cosine expansion; symmetrical hindered rotors were characterized in terms of their symmetry number, internal rotational constant, and harmonic frequency. The fitting parameters are tabulated in the Supporting Information.

For barrierless reactions, canonical variational transition state theory (CVTST) was used to locate the transition state. Because the minimum CVTST rate constant is in general located at different positions depending on the temperature, the sums of states and the microcanonical rate constants $k(E)$ vary with temperature. The $k(E)$ values computed using this approximation are not as accurate as those obtained using full microcanonical VTST (μVTST),[61−63] but trial calculations on this and similar reactions suggest that the results probably agree to within a factor of ~2 with those obtained using a full μVTST treatment. This level of accuracy is sufficient for the present purposes, considering the expected errors in the computed thermochemistry.

The following procedure was used to carry out the CVTST calculations. The reaction path was assumed to correspond to a bond being formed or broken. Constrained geometry optimizations were carried out at a series of fixed bond distances; the optimized geometries were used to obtain the rotational constants. At each fixed bond distance, a vibrational analysis was carried out to obtain the projected harmonic vibrational frequencies orthogonal to the reaction coordinate.[64] The vibrational ZPE from the orthogonal modes, $\Delta E_z(s)$, and the electronic energy $\Delta U(s)$ at each fixed bond distance s were used to compute the potential energy with ZPE corrections: $V(s) = \Delta U(s) + \Delta E_z(s)$, where $\Delta U(s) = U(s) - U(s{=}0)$ and $\Delta E_z(s) = E_z(s) - E_z(s{=}0)$. The partition functions in eq 1 were computed using the rotational constants and the vibrational frequencies for the orthogonal normal modes evaluated at the fixed distance s. The CVTST rate constant for a given temperature is identified as the minimum "trial" CTST rate constant as a function of distance along the reaction coordinate: $k^{CVTST}(T) = \min k^{CTST}(T,s)$, where $k^{CTST}(T,s)$ is the canonical TST rate constant given by eq 1 with $\Delta E_0^{\ddagger}(T)$ replaced by $V(s)$.[62,65,66]

For pressure-dependent reactions and reaction systems consisting of multiple isomers, the MultiWell ME code was used. The MultiWell ME code employs RRKM theory[58] to compute energy-dependent microcanonical rate constants for reactions with intrinsic energy barriers; the energy-dependent specific unimolecular rate constant $k(E)$ for a unimolecular reaction is given by

$$k(E) = L^{\ddagger} \times \frac{1}{h} \frac{G^{\ddagger}(E - E_0)}{\rho(E)} \quad (2)$$

where $G^{\ddagger}(E{-}E_0)$ is the sum of states for the transition state, E_0 is the reaction critical energy, and $\rho(E)$ is the density of states of the reactant molecule. The sums and densities of states were computed using the Stein−Rabinovitch extension[67] of the Beyer−Swinehart algorithm,[68] which is implemented in the DenSum code (MultiWell Program Suite).

The temperature- and pressure-dependent rate constants were obtained using the MultiWell ME code. N_2 gas was used as the bath gas, and the energy transfer was treated using the conventional exponential-down model with $\langle \Delta E \rangle_{down} = 200(T/300\ K)^{0.85}\ cm^{-1}$.[38,65,66,69] The Lennard-Jones parameters for N_2 gas (σ = 3.74 Å and ε/k_B = 82 K) were taken from the literature.[70] The Lennard-Jones parameters for all of the wells (σ = 4.94 Å and ε/k_B = 275 K) were based on those estimated by Golden for the $HOCH_2CH_2$ intermediate.[36] The pressure-dependent total rate constants $k^{rec}(T,M)$ for OH + reactant were calculated using

$$k^{rec}(T,M) = k_{\infty}^{rec}(T)[1 - f_{OH+reactant}] \quad (3)$$

where $k_{\infty}^{rec}(T)$ is the high-pressure-limit rate constant for the combination reaction and $f_{OH+reactant}$ is the fractional yield of reactants.[20] The initial energy distribution for the simulations was the chemical activation distribution for the combination reaction producing the prereactive complex. The rate constants for OH + CH_2O and OH + CH_2NH were calculated over the temperature range from 100 to 1000 K at N_2 pressures from 0.001 to 10 atm. For OH + CH_2CH_2, the simulations were carried out for temperatures ranging from 100 to 2000 K at N_2 pressures from 0.001 to 100 atm.

All of the parameters needed to reproduce the calculations are given in the Supporting Information. Energies are expressed in units of hartrees or kcal mol^{-1}, unimolecular rate constants in units of s^{-1}, and bimolecular rate constants in units of cm^3 $molecule^{-1}$ s^{-1}.

3. RESULTS AND DISCUSSION

For all three systems, both addition and abstraction reactions were investigated. Details of the reaction pathways are

DOI: 10.1021/acs.jpca.5b00910
J. Phys. Chem. A 2015, 119, 7578−7592

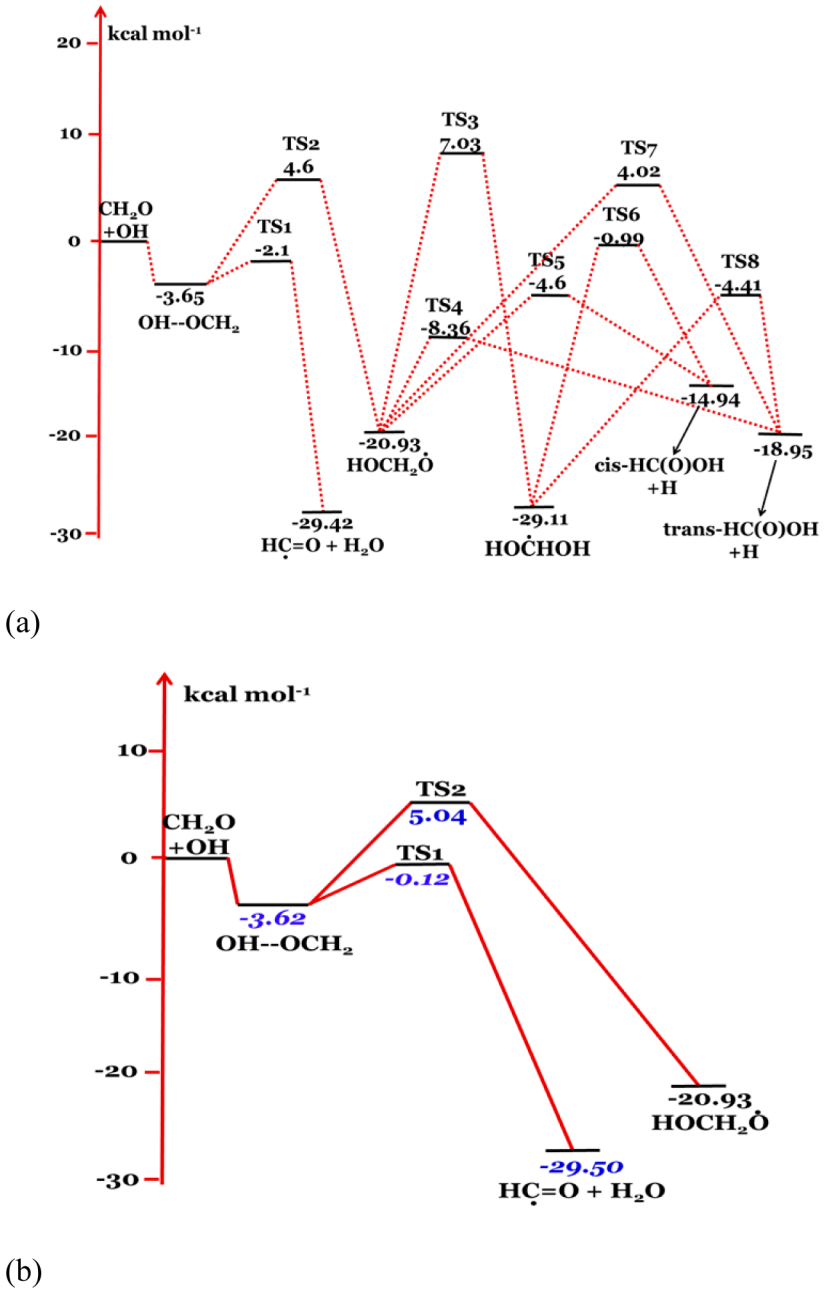

Figure 1. Potential energy surface for the OH + CH_2O reaction obtained using (a) CC-a//BH-a (values shown in black) and (b) CC-a//CC-a (values shown in blue). The relative energies include ZPE corrections.

presented in section 3.1, enthalpies of reaction in section 3.2, and rate constants in section 3.3.

3.1. Reaction Pathways. *3.1.1. OH + CH_2O.* The PES for the OH + CH_2O reaction system is shown in Figure 1. Energies of the stationary points were obtained using CC-a//BH-a and CC-a//CC-a. The ZPE-corrected energies of the complex, intermediates, and products are shown relative to the energy of the reactants. The reaction of OH with CH_2O is found to occur via a van der Waals complex with C_s symmetry in which the H atom in OH points toward the O atom in CH_2O (Figure 1). The two levels of theory give computed binding energies of 3.65 kcal/mol (CC-a//BH-a) and 3.62 kcal/mol (CC-a//CC-a), which are mutually consistent and in good agreement with that of Xu et al.,[27] who reported a value of 3.6 kcal/mol (at the CCSD(T)/6-311+G(3df,2p)//CCSD/6-311++G(d,p) level of theory). To extract an aldehydic H atom, starting from the prereactive complex, the OH rotates in the plane until the O atom comes close to the aldehydic H atom to pass through the geometry of TS1. The computed barrier heights for abstraction are 1.5 kcal/mol (CC-a//BH-a) and 2.5 kcal/mol (CC-a//CC-a). The energy difference of ∼1 kcal/mol is due to differences in the geometries and frequencies obtained using the two levels of theory (given in the Supporting Information). Comparing the BH-a and CC-a levels of theory for the C_1--H_3--O_5 bond lengths in TS1, we find values of 1.176 Å versus 1.142 Å, respectively, for C_1--H_3 and 1.415 Å versus 1.573 Å, respectively, for H_3--O_5). Moreover, the imaginary frequency in TS1 (which affects tunneling) also differs by ∼450 cm^{-1} when computed using the two levels of theory.

To form a new C−O bond between the C atom in formaldehyde and the O atom in OH, the hydroxyl radical must

DOI: 10.1021/acs.jpca.5b00910
J. Phys. Chem. A 2015, 119, 7578−7592

move out of plane to pass through the nonplanar geometry of TS2. This results in a considerable energy penalty. The barrier height for addition to the sp^2 carbon atom is 8.6 kcal/mol when computed using CC-a//CC-a, in good agreement with the value of 9.3 kcal/mol reported by Xu et al.[27] In contrast, the barrier height computed using CC-a//BH-a is significantly higher than that computed using CC-a//CC-a. These differences are due to differences in the vibrational frequencies and spatial symmetries of the optimized geometries, which may also explain the large differences in barrier heights reported in the literature for different levels of theory.[27,28] The discrepancies among different levels of theory are discussed in the Supporting Information (page 69). In addition, we also computed the CCSD(T) energy by using the "GUESS=MIX" keyword. The corrected energy of 8.4 kcal/mol (at the CC-a//BH-a level) is in very good agreement with the CC-a//CC-a value in the present work and with the value reported by Xu et al.[27] The $HOCH_2O$ intermediate can isomerize by migration of H to form HOCHOH, which can react further, ultimately dissociating to produce *cis*- and *trans*-HC(O)OH + H. The intervening intermediates and transition states were optimized only at the CC-a//BH-a level of theory because the first barrier is high, which makes these pathways negligible under the conditions considered in this work.

3.1.2. OH + CH_2CH_2. Stationary points on the PES for the OH + CH_2CH_2 reaction are shown in Figure 2. The relative

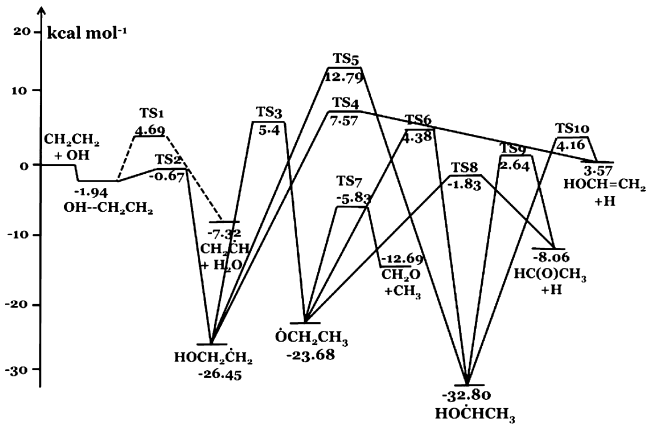

Figure 2. Potential energy surface for the OH + CH_2CH_2 reaction obtained using CC-a//BH-a. The relative energies include ZPE corrections.

energies include ZPE corrections. The reaction proceeds via the formation of a prereactive complex with C_{2v} symmetry in which the OH group is perpendicular to the C=C bond (Figure S5 in the Supporting Information). The prereactive complex is 1.94 kcal mol^{-1} lower in energy than the reactants, in good agreement with the results of previous studies.[37−39] The IRC calculations using BH-a predict that both the addition and H-abstraction reaction channels proceed via the same prereactive complex. This result differs from that reported by Senosiain et al.[38] at the RQCIST/QCI level of theory, which predicts that only the addition reaction proceeds through a prereactive complex. The latter result can be replicated using the B3LYP/aug-cc-pVTZ method, which involves a different density functional (as shown in this work). The fact that minor differences in the level of theory can result in the identification of two distinct reaction paths suggests that both pathways exist on the PES, i.e., at the B3LYP level, IRC calculations suggest that TS1 → CH_2CH_2 + OH, whereas at the BH-a level, TS1 → OH--CH_2CH_2. The abstraction barrier heights (measured from the prereactive complex) computed using CC-a//BH-a are within ∼1 kcal/mol of the results reported by Greenwald et al.,[37] Senosiain et al.,[38] and Zhu et al.[40] A complete summary of the thermochemistry computed in the present work and reported in the literature is presented in section 3.2.

3.1.3. OH + CH_2NH. The stationary points on the PES for OH + CH_2NH (obtained using CC-a//BH-a or CC-a/CC-a) are shown in Figure 3. As described in more detail in section 3.3, the OH radical approaches from long distance with its H atom pointed toward the lone pair on the N atom of CH_2NH. It forms a stable planar prereactive complex with C_s symmetry (Figure S9 in the Supporting Information). The computed energy of the complex is 5.37 kcal/mol (CC-a//BH-a) or 4.74 kcal/mol (CC-a//CC-a) lower than the energy of the reactants. These values are reasonably consistent with each other and with the value of 5.9 kcal/mol computed by Bunkan et al.[17] at the CC-pQ//CC-p level of theory. The N--H−O bond, which is responsible for the binding energy, is stronger than the O--H−O bond formed in the OH + CH_2O reaction (∼3.6 kcal/mol).

IRC calculations show that in order for H abstraction to occur, the OH in the prereactive complex must rotate until the O atom approaches any one of the three H atoms in the CH_2NH moiety; the three H atoms reside in three unique structural environments. The transition-state structure for H abstraction from one C−H bond is planar (C_s symmetry) while that from the other C−H bond is nonplanar (C_1 symmetry). IRC calculations show that H abstraction from the N−H bond is not in the CH_2NH molecular plane, and the nonplanar transition state structure has C_1 symmetry.

As measured from the prereactive complex, the barrier heights for hydrogen abstraction from the *cis*- and *trans*-C−H bonds and from the N−H bond are 6.3, 4.4, and 3.11 kcal/mol, respectively, at the CC-a//BH-a level of theory. At the CC-a//CC-a level, the respective values are 6.4, 5.4, and 4.1 kcal mol^{-1}. The modest energy differences using the two levels of theory are due to the slightly different geometrical parameters and zero-point energies. It should be noted that TS1 and TS3 are "emergent" (energy greater than that of the reactants) while TS2 is "submerged" (energy less than that of the reactants) using CC-a//CC-a. Bunkan et al.[17] also reported transition-state geometries similar to TS2 and TS3 at the CC-pQ//CC-p level of theory.

Not only do the H abstraction reactions proceed from the prereactive complex, but OH addition to the sp^2 carbon in CH_2NH also proceeds from the complex, forming $HOCH_2NH$, with free radical character centered mostly on the nitrogen. The addition of OH radical to the nitrogen atom to form the nitrogen−oxygen bond is less favorable, in agreement with the results of Bunkan et al.[17] The barrier heights for the addition reaction are computed to be 5.74 kcal/mol (using CC-a//CC-a) and 6.2 kcal mol^{-1} (using CC-a//BH-a). The barrier height is 3 kcal mol^{-1} lower than the barrier computed for the CH_2O + OH addition reaction and ∼1 kcal mol^{-1} higher than that computed for the OH + C_2H_4 addition reaction. The addition intermediate ($HOCH_2NH$) can follow several reaction paths leading ultimately to fragmentation products: CH_2O + NH_2, OHCHNH + H, and $OCHNH_2$ + H. These unimolecular reaction pathways are analogous to those in the OH + CH_2CH_2 reaction system. All of the transition states along these paths have a single imaginary frequency, and IRC calculations were

DOI: 10.1021/acs.jpca.5b00910
J. Phys. Chem. A 2015, 119, 7578−7592

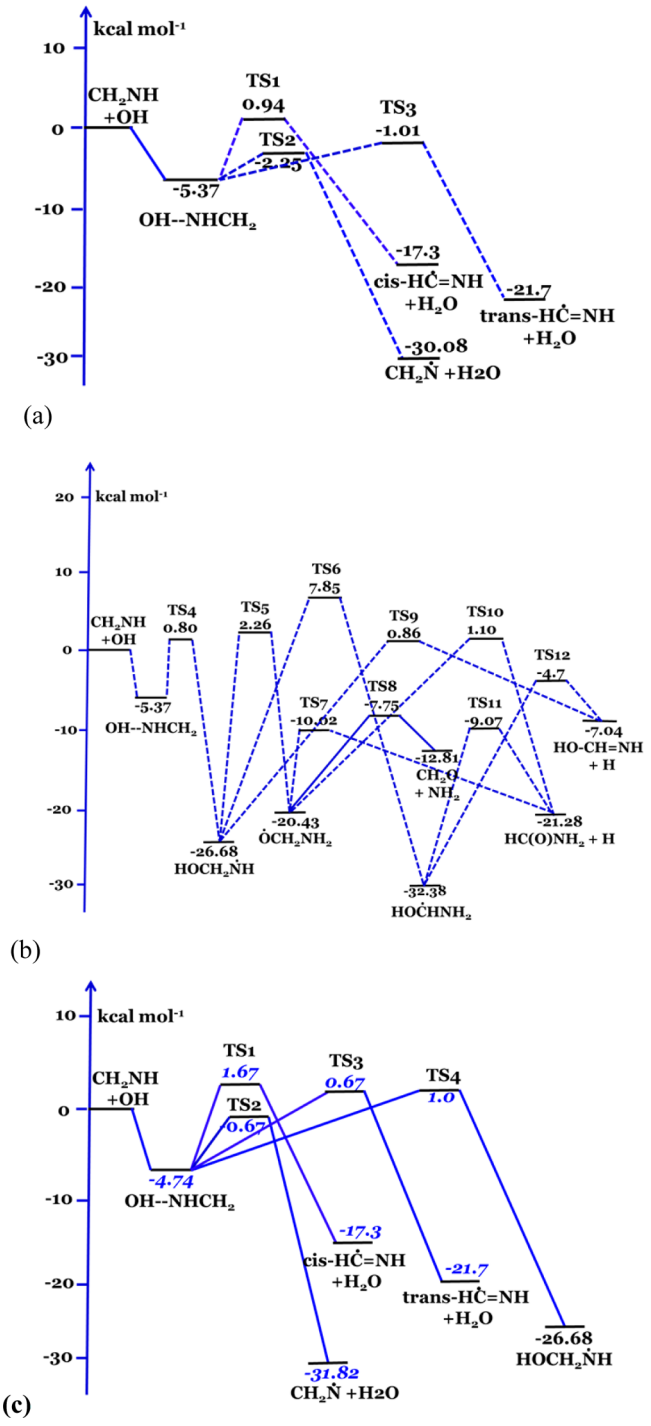

Figure 3. (a, b) Potential energy surfaces for the OH + CH_2NH obtained using CC-a//BH-a (values shown in black): (a) abstraction reactions; (b) addition reaction. (c) PES obtained using CC-a//CC-a (values shown in blue). Energies include ZPE corrections.

carried out to confirm that the transition states connect to the reactants and products indicated in Figure 3b.

3.2. Computed Enthalpies. The enthalpies relative to the reactants for the three reaction systems are given in Table 1. This table also includes some enthalpies from the Active Thermochemical Tables (ATcT),[71] which is probably the most accurate set of experimental enthalpies currently available. The enthalpies of reaction in the present work for OH + CH_2O → CHO + H_2O (computed using CC-a//CC-a) and for OH + CH_2O → HC(O)OH + H (computed using CC-a//BH-a) agree with those from the ATcT thermochemical database within ∼1 and ∼2 kcal/mol, respectively, and are in excellent agreement with the results of previous theoretical calculations. The enthalpy for OH + CH_2CH_2 → $HOCH_2CH_2$ (computed using CC-a//BH-a) agrees with the ATcT value within ∼1.5 kcal/mol. The enthalpies for the other reaction pathways for OH + CH_2CH_2 are also in excellent agreement with the experimental and theoretical values listed in Table 1. The enthalpies of reaction for the OH + CH_2NH reaction system computed in the present work are in excellent agreement with those of Bunkan et al.[17] (Table 1). These comparisons show that the CC-a//BH-a and CC-a//CC-a levels of theory are accurate to within ∼1−2 kcal/mol for these isoelectronic reaction systems.

3.3. Rate Constants and Branching Ratios. The rate constants for the three reaction systems were computed both in the high-pressure limit (CTST or CVTST methods) and as a function of pressure (RRKM/ME simulations). The computation of product branching ratios is discussed in this section. The parameters required for the kinetics calculations (total electronic energies, rotational constants, vibrational frequencies, etc.) are tabulated in the Supporting Information.

3.3.1. Transition States for Barrierless Reactions. Prereactive complexes play key roles in the three reaction systems. In each system, the entrance channel for forming the prereactive complex has no local maximum on the PES (i.e., no intrinsic energy barrier). To locate the transition state for each barrierless reaction, the potential energies (including zero-point energies of the modes perpendicular to the newly forming bond) were computed in a series of constrained optimizations as a function of the bond distance, as described in Methods. The potential energy profiles for the three entrance channels are shown in Figure 4. The geometries at some points along the reaction pathways and at the equilibrium structure of the complex for each reaction system are shown in Figure 5.

When OH radical approaches CH_2O at very long distances, the two electrostatic dipoles tend to align with the H atom in OH pointing toward the O atom in CH_2O along an extension of the CH_2O molecular axis. When they are aligned, the symmetry of the system is C_{2v}, as noted in Figure 5. As the two species approach each other, the potential energy decreases smoothly and monotonically all the way to the bottom of the potential well (Figure 4). However, the geometry of the system changes from C_{2v} to C_s at a H−O distance of 3.7 to 3.6 Å. This occurs because the C−O−O angle is 180° at long distances but begins to decrease in this distance range. Subsequently, the planar geometry (C_s symmetry) is retained until the equilibrium geometry of the prereactive complex is reached. The change in geometry from C_{2v} to C_s reflects the existence of a bifurcation in the reaction path. Outward from 3.7 Å there is just one minimum-energy path (MEP), but inward from 3.6 Å two equivalent MEPs exist, each corresponding to a minimum in the potential energy for internal rotation of the OH moiety around (approximately) the C−O axis in CH_2O. For present purposes, this is enough qualitative information for guidance in computing CVTST rate constants, but in future work we plan to examine this bifurcation in more detail.

The MEP was determined by using BH-a to compute constrained optimizations at H−O distances of 2.3 to 6.0 Å in steps of 0.1 Å. Ro-vibrational parameters were computed at each step and are presented in the Supporting Information. Figures presented in the Supporting Information show abrupt

DOI: 10.1021/acs.jpca.5b00910
J. Phys. Chem. A 2015, 119, 7578−7592

Table 1. Enthalpies of Reaction ΔH_{rxn}(0 K) (in kcal/mol)

OH + CH_2O → Products		
products	this work	literature
OH--OCH_2	−3.65,[a] −3.62[b]	−3.6,[c] −3.5[c]
$HOCH_2O$	−20.93[a]	−20.5[c]
HOCHOH	−29.11[a]	
cis-HC(O)OH + H	−14.94[a]	−16.91 ± 0.01[d]
trans-HC(O)OH + H	−18.95[a]	−20.81 ± 0.03[d]
CHO + H_2O	−29.42,[a] −29.50[b]	−29.6,[c] −30.93 ± 0.06[d]
OH + CH_2CH_2 → Products		
products	this work	literature
OH--CH_2CH_2	−1.94[a]	1.84,[e] 1.94,[f] 1.9[g]
$HOCH_2CH_2$	−26.45[a]	−27.5,[e] −31.2,[g] −28.2,[h] −24.63 ± 0.19[d]
$HOCHCH_3$	−32.80[a]	−32.7[f]
OCH_2CH_3	−23.68[a]	−22.8,[f] −23.04 ± 0.02[d]
HOCH=CH_2 + H	3.57[a]	1.0,[f] 1.28 ± 0.10[d]
$OCHCH_3$ + H	−8.06[a]	−8.8[f]
CH_2CH + H_2O	−7.32[a]	−8.30,[f] −10.4,[g] −7.95,[e] −8.58 ± 0.02[d]
CH_2O + CH_3	−12.69[a]	−16.9,[g] −12.85 ± 0.05[d]
OH + CH_2NH → Products		
products	this work	literature
OH--$NHCH_2$	−5.36,[a] −4.74[b]	−5.94[i]
$HOCH_2NH$	−26.68[a]	−27.48[i]
$HOCHNH_2$	−32.38[a]	
OCH_2NH_2	−20.43[a]	
HOCH=NH + H	−7.04[a]	
H−C(O)NH_2 + H	−21.28[a]	
CH_2N + H_2O	−30.08,[a] −31.82[b]	−30.35[i]
cis-CHNH + H_2O	−17.3,[a] −17.3[b]	−17.21[i]
trans-HCNH + H_2O	−21.7,[a] −21.7[b]	−21.75[i]
CH_2O + NH_2	−12.81	

[a]Computed using CC-a//BH-a. [b]Computed using CC-a//CC-a. [c]From Xu et al.[27] [d]From ATcT.[71] [e]From Cleary et al.[39] [f]From Senosiain et al.[38] [g]From Zhu et al.[40] [h]From Golden.[36] [i]From Bunkan et al.[17]

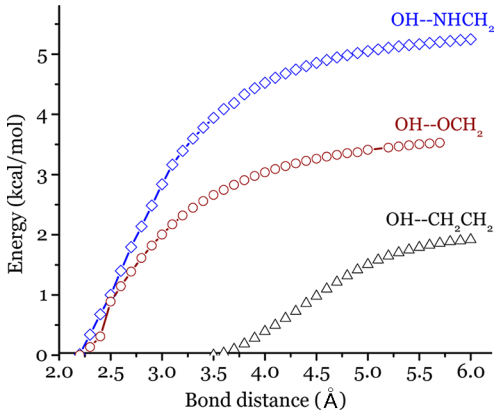

Figure 4. Potential energies (including ZPE corrections) relative to the energies of the prereactive complexes as functions of bond distance for formation of the complexes OH--OCH_2, OH--CH_2CH_2, and OH--$NHCH_2$ (obtained using CC-a//BH-a).

changes in the rotational constants and dipole moment near ≳3.6 Å, reflecting the change in geometry. Also near ≳3.6 Å, the calculated vibrational frequencies of the modes perpendicular to the reaction coordinate (assumed to be the OH−OCH_2 distance) exhibit a fluctuation, which we believe is caused by the bifurcation in the PES.

A trial CTST rate constant was computed at each point along the reaction path using the ro-vibrational parameters. The sets of trial rate constants computed at 200, 300, and 400 K for OH + CH_2O are shown in Figure 6a. At each temperature, the plot shows two minima, an effect that is the result of the changes in the rotational constants and vibrational frequencies. Thus, a two-transition-state (2-TS) model is needed to describe this single entrance channel, even though the potential energy plot in Figure 4 is smooth and monotonic. Multiple-transition-state models are well-known (examples have been discussed by Greenwald et al.[37] and Senosiain et al.[38]). According to Miller,[72] the effective sum of states $G^{\ddagger}_{eff}$ to be used in eq 2 for a 2-TS model is given by

$$\frac{1}{G^{\ddagger}_{eff}(E)} = \frac{1}{G^{\ddagger}_{a}(E)} + \frac{1}{G^{\ddagger}_{b}(E)} \quad (4)$$

where $G^{\ddagger}_{a}$ and $G^{\ddagger}_{b}$ are the sums of states (evaluated at the same zero of energy) for transition states a and b. For this particular association reaction, both transition states are variational, and the outer and inner transition states correspond to the C_{2v} and C_s symmetry regimes (see Figure 6a).

The MEP in the entrance channel for formation of the OH--CH_2CH_2 complex was located by carrying out constrained optimizations using BH-a at O−C distances from 3.5 to 6.0 Å with a step size of 0.1 Å. The potential energy along the MEP is shown in Figure 4. This complex is very well known in the literature,[36−40] but the predicted symmetry depends on the level of theory. At the QCISD(T) level of theory, the prereactive complex has C_s symmetry, as reported by Senosiain et al.,[38]

DOI: 10.1021/acs.jpca.5b00910
J. Phys. Chem. A 2015, 119, 7578−7592

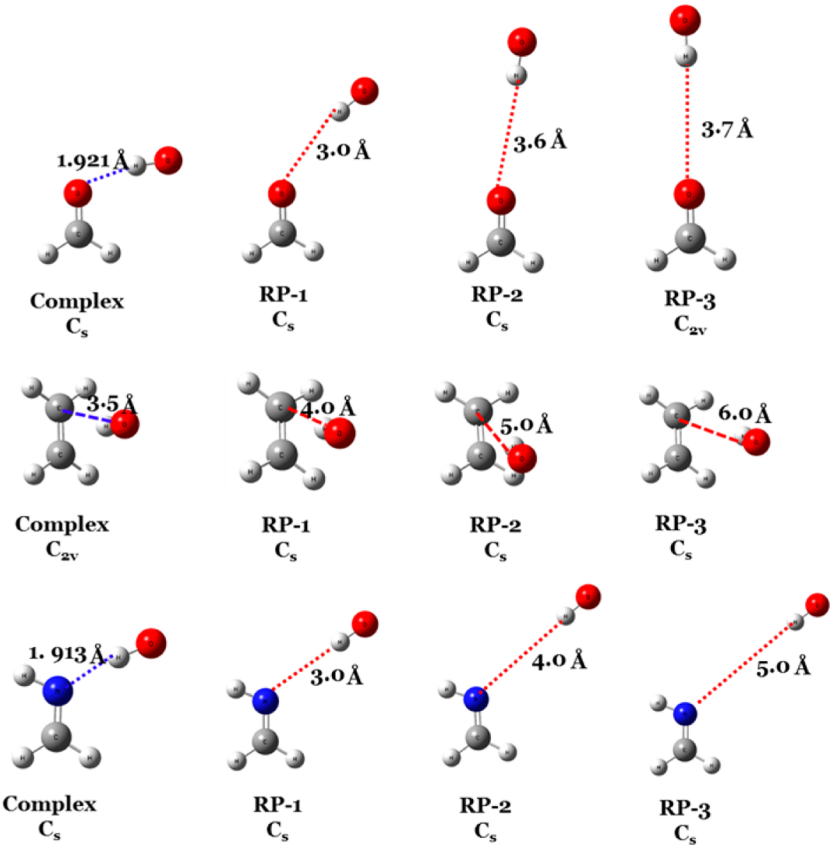

Figure 5. Optimized geometries of the prereactive complex and at several points along the reaction pathway for each entrance channel. The symmetry label (C_{2v} or C_s) is given for each geometry.

but in the present work using BH-a, the equilibrium structure was found to have C_{2v} symmetry. However, this is true only at the equilibrium position. At longer distances along the MEP, BH-a predicts that the system has C_s symmetry, since the O atom is slightly displaced from the center line of the C═C double bond (see Figure 5). In this case, the change from C_s to C_{2v} symmetry occurs at the equilibrium geometry of the complex and does not affect the rate constants, unlike the case of the OH + CH_2O reaction. The ro-vibrational parameters as functions of bond distance and related information are given in the Supporting Information. The trial rate constants as a function of bond distance, shown in Figure 6b, exhibit only one minimum at each temperature.

The MEP in the entrance channel for the formation of the OH--CH_2NH prereactive complex is predicted by BH-a to have C_s symmetry at all distances, including the equilibrium structure (see Figure 5). The computed ro-vibrational parameters as functions of the H−N bond distance are tabulated in the Supporting Information. The trial CTST rate constants, shown in Figure 6c, exhibit a single minimum at each temperature, calling for a single-transition-state model. The CVTST rate constant calculated in the present work is only about one-half of the value obtained by Bunkan et al.,[17] who used the long-range TST model of Georgievskii and Klippenstein.[18] Both sets of calculated values are given in Table 2.

3.3.2. OH + CH_2O Reaction System. ME simulations were used to calculate the temperature- and pressure-dependent rate constants shown in Figure 7 for temperatures from 200 to 400 K (at 1 atm N_2). Also shown are data from experimental and theoretical studies.[23−31] The rate constants computed using CC-a//BH-a exhibit a very weak pressure dependence, consistent with the results of previous studies,[23−25] and a distinct *negative* temperature dependence. However, the rate constants computed using CC-a//CC-a exhibit a weakly *positive* temperature dependence. The rate constants using CC-a//BH-a and CC-a//CC-a differ by at least a factor of 10 because of the different computed barrier heights and partition functions, as discussed in section 3.1.1.

Recently, Zhang et al.[28] calculated the rate constant using CCSD(T)//MP2(Full) + ZPE × 0.95 with the 6-311++G(df,pd) basis set and obtained a value of 36.9×10^{-12} cm^3 $molecule^{-1}$ s^{-1} at 298 K. Their result is 4 times larger than the experimentally measured value[23−25] of 9.0×10^{-12} cm^3 $molecule^{-1}$ s^{-1}. This large difference is partly due to the fact that their rate constant is based on the expression $k = k_1k_2/(k_{-1} + k_2)$ and the assumption that $k_{-1} \gg k_2$. This assumption may not be correct, however, as suggested by Greenwald et al. in their paper on the OH + CH_2CH_2 reaction.[37] Furthermore, the barrier heights calculated using the MP2 level of theory may not be sufficiently accurate. Xu et al.[27] used CCSD(T)//B3LYP with the 6-311++G(d,p) basis set and obtained a rate constant with a very strong negative temperature dependence and a magnitude about twice as high as that of the experimental value at 298 K (Figure 7).[23−25] Neither of these groups reported changes in the reaction path geometry or any consideration of multiple transition states along the reaction path.

The rate constants calculated using CC-a//CC-a in the present work are in good agreement with the experimental values.[23−25,31] The calculated temperature dependence is only

DOI: 10.1021/acs.jpca.5b00910
J. Phys. Chem. A 2015, 119, 7578−7592

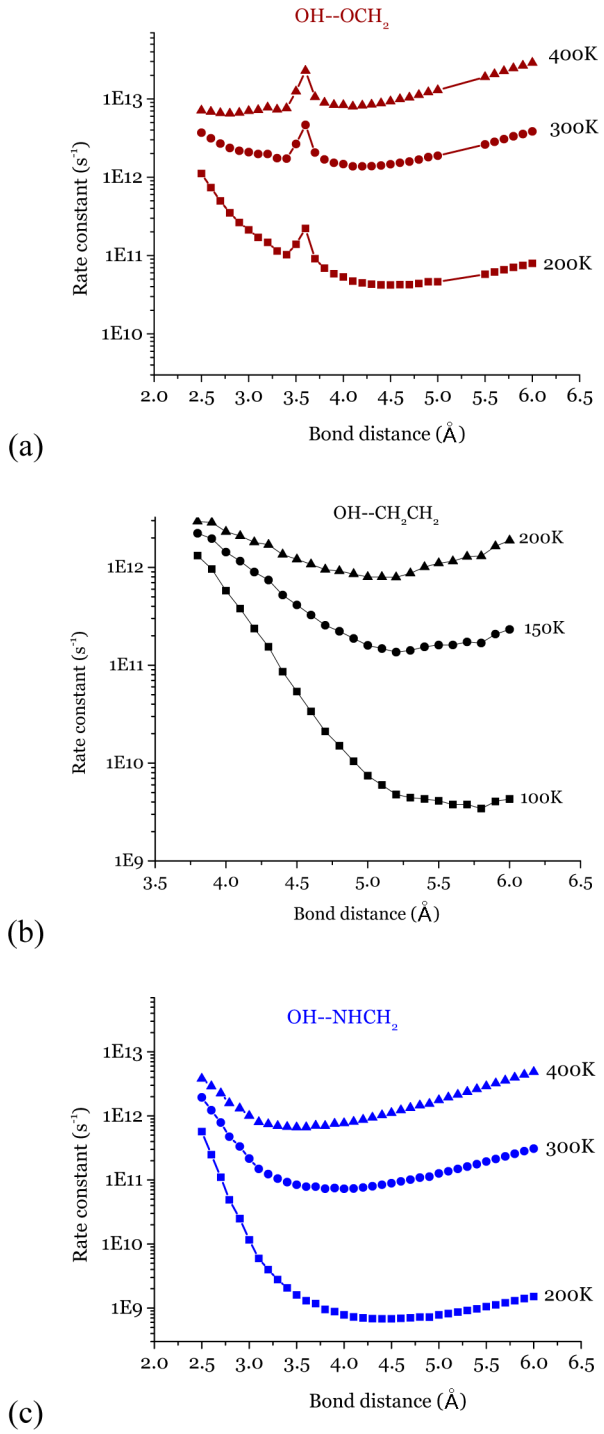

Figure 6. Trial CTST rate constants for dissociation via the entrance channels as functions of bond distance (CC-a//BH-a level of theory): (a) CH_2O + OH channel; (b) CH_2CH_2 + OH channel; (c) CH_2NH + OH channel.

slightly stronger than in the experiments, and the magnitude is within a factor of 2 to 3 over the entire temperature range from 200 to 400 K. Adjusting the barrier height of TS1 by −0.3 kcal/mol, which is well within the estimated accuracy of the theoretical methods (~2 kcal/mol),[5,38] brings the computed rate constants into almost exact agreement with the experimental values over the entire temperature range.[23−25,31] If a 2-TS model had not been used, the computed rate constants would have been about twice as large as the experimental values.

Table 2. Capture Rate Constants (in Units of 10^{-10} cm^3 $molecule^{-1}$ s^{-1}) for the OH + CH_2NH Entrance Channel

T (K)	Bunkan et al.[17,a]	this work[b]
100	5.83	2.51
200	5.19	2.47
225	5.09	2.40
250	5.00	2.35
275	4.93	2.35
300	4.85	2.34
325	4.79	1.91
350	4.73	1.90
375	4.68	2.28
400	4.63	2.28

[a]Based on long-range transition state theory.[18] [b]Calculated using the CVTST method.

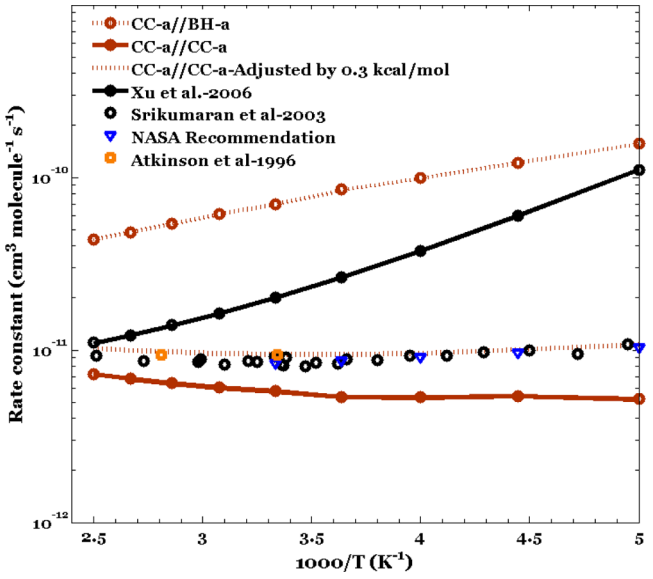

Figure 7. Plots of total rate constants (in cm^3 $molecule^{-1}$ s^{-1}) for OH + CH_2O vs $1000/T$ at 1 atm pressure.

3.3.3. OH + CH_2CH_2 Reaction System. Figure 8 presents the calculated rate constants for production of C_2H_4OH as a function of $1000/T$ over the temperature range from 200 to 400 K at 1 atm and compares them with the NASA recommendations[31] and the results of other theoretical calculations.[36−39] The rate constants computed in the present work at 298 K are a factor of ~2 smaller than those of Golden,[36] Greenwald et al.,[37] and Senosiain et al.[38] At higher temperature, the present rate constants are in good agreement with those reported by Cleary et al.[39] With a small energy adjustment (−0.3 kcal/mol), the rate constant at 298 K and 1 atm is brought into very good agreement with the results of Golden,[36] Greenwald et al.,[37] Senosiain et al.,[38] and Cleary et al.[39] The temperature dependence is most similar to that of Greenwald et al.[37] The present rate constants with and without adjustment at 300 K are also in good agreement with the experimental values.[29,32,34,35]

As suggested by Tully[33] and supported by Senosiain et al.,[38] the hydrogen abstraction pathways in the OH + CH_2CH_2 reaction system are important at higher temperatures. We calculated the high-pressure-limit rate constants using CTST for OH + C_2H_4 → C_2H_3 + H_2O with and without adjustment of barrier heights, and the results are shown in Figure 9.

DOI: 10.1021/acs.jpca.5b00910
J. Phys. Chem. A 2015, 119, 7578−7592

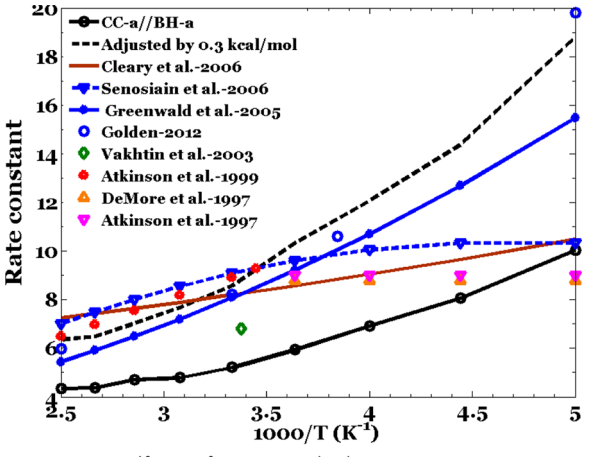

Figure 8. Plots of rate constants (in units of 10^{-12} cm^3 molecule^{-1} s^{-1}) for the OH + CH_2CH_2 addition reaction vs 1000/T at 1 atm pressure.

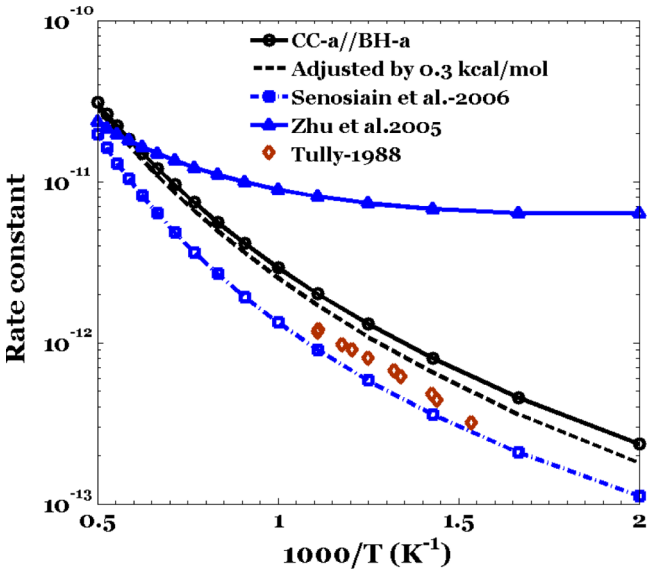

Figure 9. High-pressure-limit rate constants (in cm^3 molecule^{-1} s^{-1}) for H abstraction in the OH + CH_2CH_2 system.

The present rate constant with an adjustment of +0.6 kcal/mol in transition state TS2 is in good agreement with the experimental results of Tully.[33] This adjustment is well within the estimated accuracy of the theoretical methods (~2 kcal/mol).[5,38] The present rate constant without adjustment is also in good agreement with the one computed by Senosiain et al.,[38] who empirically adjusted their computed barrier height by +0.4 kcal/mol. Zhu et al.[40] computed rate constants at least 10 times higher than the experimental values[33] because their computed barrier height was too low.[40]

To understand the effect of temperature on the branching ratios, the addition, abstraction, and elimination product yields were calculated over the temperature range from 100 to 2000 K at 1 atm. The branching ratios for different products as functions of temperature are given in the Supporting Information. At 900 K, the branching ratios show equal contributions from formation of $HOCH_2CH_2$ and dissociation to CH_2CH + H_2O. The hydrogen abstraction channel dominates above >900 K at 1 atm. This result is in good agreement with that of Senosiain et al.[38] The branching ratios reported by Cleary et al.[39] and Zhu et al.[40] show equal contributions at 750 and 1000 K, respectively. The differences among these studies may be due to different computed barrier heights. We found that OH addition followed by CH_3 elimination is the dominant reaction pathway between 295 and 600 K; H atom elimination is largely insignificant at the lowest temperatures, in agreement with the results of Senosiain et al.[38]

3.3.4. OH + CH_2NH Reaction System. Figure 10 shows the rate constants for the formation of *cis*- and *trans*-HC═NH + H_2O

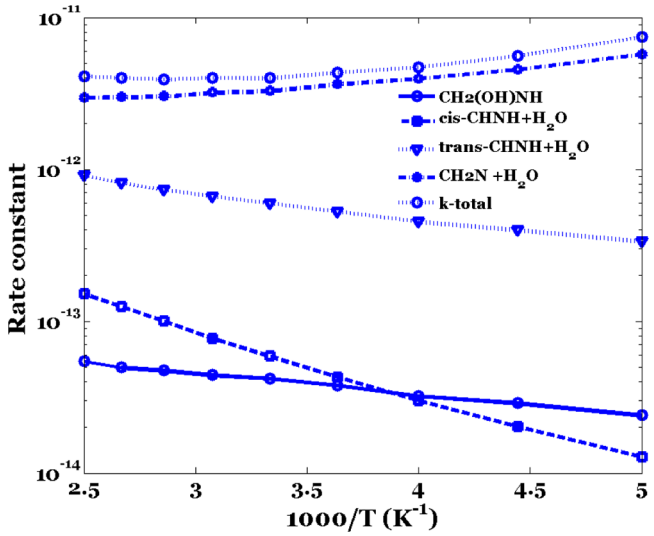

Figure 10. Rate constants (in cm^3 molecule^{-1} s^{-1}) for various OH + CH_2NH reaction channels as functions of 1000/T at 1 atm pressure (calculated using CC-a//CC-a).

(hydrogen abstraction), CH_2N + H_2O (hydrogen abstraction), and $HOCH_2NH$ (addition) as functions of temperature (200−400 K) at 1 atm. The calculations predict that hydrogen abstraction from the N−H bond is favored over abstraction from the C−H bonds. This is mostly due to the fact that hydrogen abstraction from the N−H bond has the lowest barrier (Figure 3). The addition reaction is at least 2 orders of magnitude slower than N−H abstraction and 1 order of magnitude slower than abstraction of a methylenic H atom to form the *trans*-HC═NH product. Again, this is a consequence of the relative barrier heights. These results are similar to those of Bunkan et al.,[17] who carried out calculations at the CC-pQ//CC-p level of theory. The total rate constant in our study at 300 K and 1 atm, 4.0×10^{-12} cm^3 molecule^{-1} s^{-1} at the CC-a//CC-a level of theory, is in good agreement with the value of 3.0×10^{-12} cm^3 molecule^{-1} s^{-1} computed by Bunkan et al.[17]

As discussed above, minor adjustment of the barrier heights for the OH + CH_2O and OH + CH_2CH_2 reactions resulted in excellent agreement with the experimental data. Without adjustment, the agreement with experiments was good, but adjustment gave better agreement. This suggested that for this isoelectronic reaction system, a similar adjustment should lead to improved predictions. Therefore, we adjusted the barrier height of the OH + CH_2NH inner channel by −0.3 kcal/mol, the same as the empirical adjustments to the lower-energy pathways in the other two systems. This adjustment is well within the estimated accuracy of the theoretical methods (~1−2 kcal/mol), as discussed above. The rate constants obtained using the adjusted barrier height (decreased by 0.3 kcal/mol) as a function of temperature and pressure are shown in Figure 11.

DOI: 10.1021/acs.jpca.5b00910
J. Phys. Chem. A 2015, 119, 7578−7592

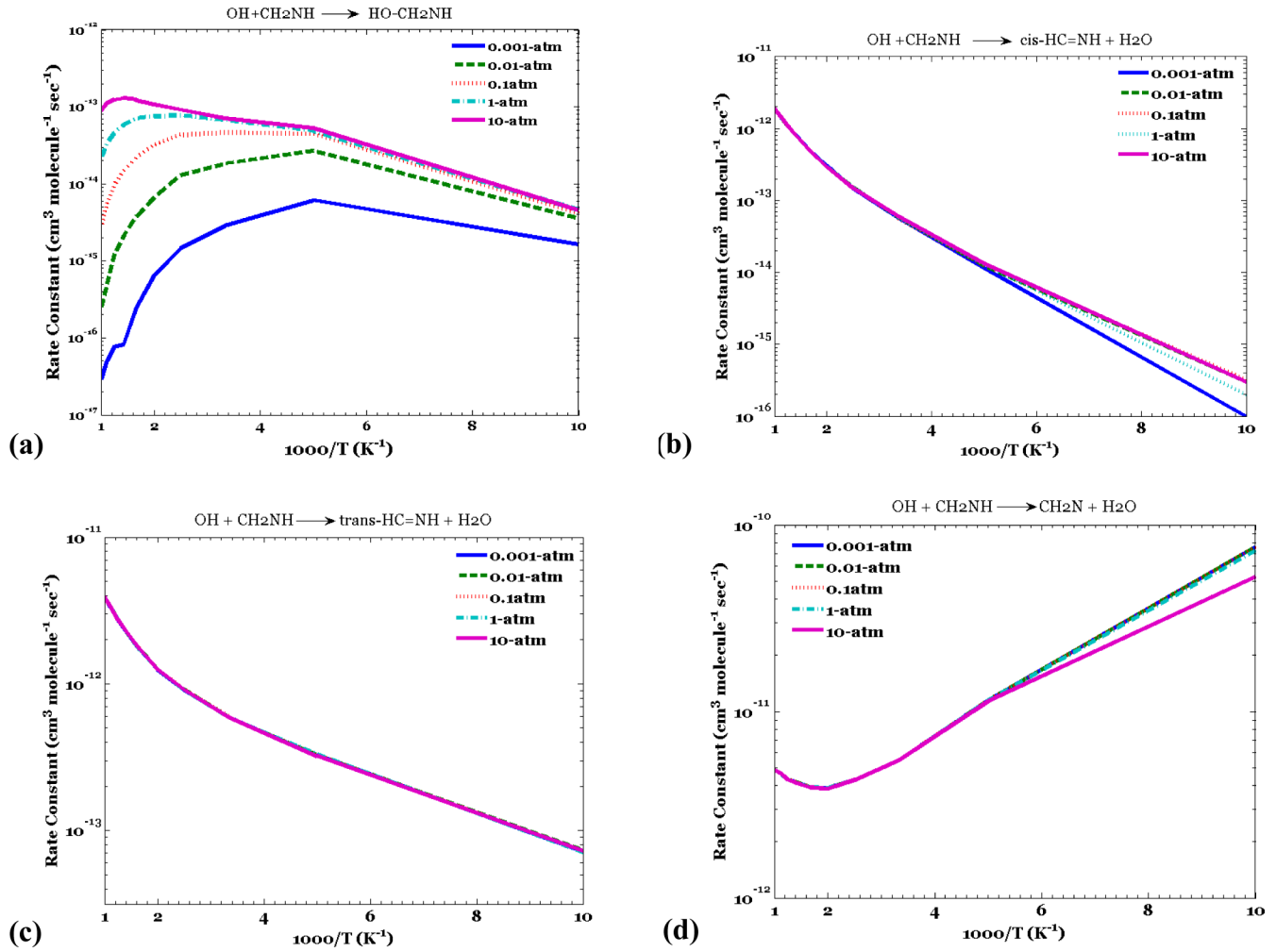

Figure 11. Calculated rate constants for OH + CH_2NH → products over the temperature range from 100 to 1000 K at different pressures.

The rate constants without adjustment are given in the Supporting Information.

Figure 11 shows that the rate constant for the formation of the OH--CH_2NH prereactive complex is distinctly pressure-dependent, in contrast to those for the abstraction reactions, which are not, as expected. The pressure dependence of the addition reaction is more prominent at higher temperatures, where pressure falloff is more important; at lower temperatures, the reaction is closer to its high-pressure limit.

The abstraction reactions show a weaker pressure dependence than the addition reaction. The pressure dependence is not completely absent, as it would be in a simpler reaction system, but it is finite because all of the abstraction reactions proceed via the prereactive complex, which can undergo collisional stabilization. The abstraction reactions that produce *cis*-HC═NH + H_2O and CH_2N + H_2O exhibit a weak pressure dependence at low temperatures, while the reaction producing *trans*-CH═NH + H_2O is almost completely independent of pressure. These results are consistent with those of Bunkan et al.[17]

The weak pressure dependence in two of the OH + CH_2NH H abstraction reactions is similar to that observed in the OH + CH_2O reaction. The OH + CH_2NH addition reaction is distinctly pressure-dependent, similar to the OH + CH_2CH_2 addition reaction. The total rate constants for the isoelectronic reactions OH + CH_2NH, OH + CH_2O, and OH + CH_2CH_2 computed with and without adjustment of barrier heights are discussed in section 3.4. It is clear that the total rate constant for OH + CH_2NH has similarities to both of its cousins.

Figure 12 shows the branching ratios for the formation of $HOCH_2NH$, *cis*- and *trans*-HC═NH + H_2O, CH_2N + H_2O, and HOHC═NH + H. The branching ratios are tabulated in the Supporting Information. It is clear from the figure that the unadjusted and adjusted simulations give approximately the same product ratios at higher temperatures, but at lower temperatures the yields of the prereactive complex and CH_2N + H_2O are more significant. These changes are qualitatively consistent with what would be expected considering the adjustment of −0.3 kcal/mol.

As the temperature increases, the yields of both the prereactive complex and CH_2N + H_2O decrease. The branching ratios of *cis*-HC═NH and *trans*-CHNH increase with temperature. Recently, Bunkan et al.[17] calculated the branching ratios at 298 K for the formation of $HOCH_2NH$ (4%), *cis*-HC═NH (12%), *trans*-HC═NH (36%), and CH_2N + H_2O (49%) at 298 K and 1 atm pressure. The corresponding branching ratios in the present work are 1%, 1%, 9% and 87%, respectively. The differences between the two studies are due to both the different reaction paths (via the prereactive complex or not) and differences in the computed barrier heights. In both calculations, the formation of $OHCH_2NH$ and the formation of HOHC═NH + H are almost negligible compared with the

DOI: 10.1021/acs.jpca.5b00910
J. Phys. Chem. A 2015, 119, 7578−7592

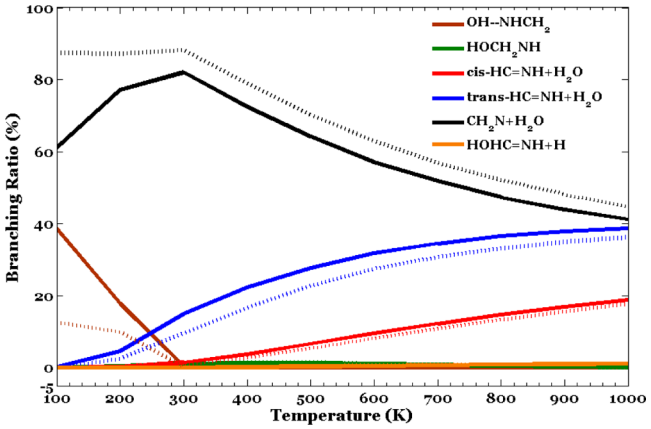

Figure 12. Calculated branching ratios as functions of temperature at 1 atm for two sets of data: (1) without adjustment of the barrier height (solid lines); (2) with the barrier height decreased by 0.3 kcal/mol (dashed lines).

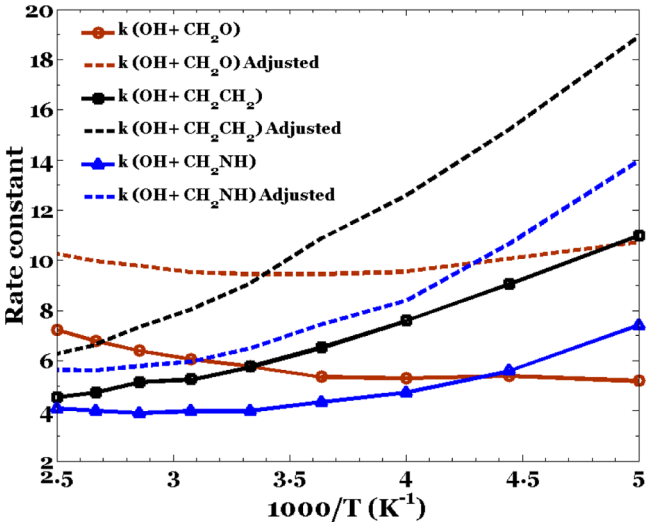

Figure 13. Rate constants (in units of 10^{-12} cm^3 molecule^{-1} s^{-1}) for the OH + CH_2O (brown), OH + CH_2CH_2 (black), and OH + CH_2NH (blue) reactions as functions of $1000/T$ at 1 atm pressure (1) without adjustment of the barrier heights (solid lines) and (2) with the barrier heights decreased by 0.3 kcal/mol (dashed lines).

abstraction reactions. At T > 1000 K, hydrogen abstraction from the C−H bonds is dominant over abstraction from the N−H bond.

3.4. Comparison of Rate Constants. The total rate constants for OH + CH_2NH and the isoelectronic systems OH + CH_2O and OH + CH_2CH_2 with and without adjustment of barrier heights are shown in Figure 13 and given in Table 3. At higher temperatures, the rate constant for OH + CH_2NH is close to the value for OH + CH_2CH_2. This result is true both with and without adjustment of barrier heights. At lower temperatures, the rate constant for the OH + CH_2NH reaction is closer to the rate constant for OH + CH_2O in both simulations. The OH + CH_2NH reaction system has similarities to both the OH + CH_2O and OH + CH_2CH_2 reaction systems.

How reliable are these predicted rate constants for the OH + CH_2NH system? As discussed in previous sections, the theoretical methods are accurate to ∼2 kcal/mol when evaluated using large databases consisting of a wide variety of chemical species.[5,38] In this specific application to the isoelectronic OH + CH_2O and OH + CH_2CH_2 reactions, the reaction enthalpies are accurate to ∼1−2 kcal/mol, and the computed and experimental total rate constants at ≥300 K are in good agreement with no barrier height adjustments and can be brought into excellent agreement when a correction of only −0.3 kcal/mol is applied in each case. The same adjustment was applied to OH + CH_2NH because it is isoelectronic with the others. There is no certainty that the −0.3 kcal/mol correction is equally valid for all three reaction systems, but it seems likely that the error is substantially less than the nominal average error of ∼2 kcal/mol found for large databases. In light of these considerations, we estimate that the relative error is no greater than ∼2 kcal/mol and is probably of the order of 0.5 kcal/mol, which results in a factor of ∼2 uncertainty in the predicted total rate constants near 298 K.

4. CONCLUSIONS

A number of conclusions can be reached as a result of the present work. The three isoelectronic reaction systems behave similarly. For the OH + CH_2O and OH + CH_2CH_2 reaction systems, the quantum-chemistry methods perform quite well for reaction enthalpies, with errors of ∼1−2 kcal/mol, and even better for the energies of low reaction barriers.

The geometries computed using BH-a and CC-a were very similar for stable species but were significantly different for transition states. The same was true for harmonic vibrational frequencies. This observation calls into question the utility of using a low level of theory (like DFT) followed by single-point calculations at a higher level of theory (a "low/high" strategy). Our calculations suggest that although they are expensive, fully ab initio methods like CCSD(T) with large basis sets are still

Table 3. Calculated Total Rate Constants (in Units of 10^{-12} cm^3 molecule^{-1} s^{-1}) for the Three Reactions with and without a Barrier Height Adjustment of −0.3 kcal/mol

	OH + CH_2O		OH + CH_2CH_2		OH + CH_2NH	
T (K)	unadjusted	adjusted	unadjusted	adjusted	unadjusted	adjusted
200	5.20	10.7	11.0	18.9	7.42	14.0
225	5.40	10.1	9.06	15.2	5.60	10.7
250	5.31	9.55	7.59	12.6	4.73	8.40
275	5.36	9.46	6.53	10.9	4.34	7.46
300	5.77	9.45	5.76	9.11	4.00	6.51
325	6.06	9.54	5.26	8.06	4.01	5.97
350	6.40	9.78	5.15	7.37	3.92	5.80
375	6.79	9.98	4.74	6.65	4.01	5.63
400	7.23	10.3	4.55	6.30	4.11	5.64

DOI: 10.1021/acs.jpca.5b00910
J. Phys. Chem. A 2015, 119, 7578−7592

needed to achieve energies accurate to $\lesssim$2 kcal/mol. When less accuracy is tolerable, the low/high strategy performs reasonably in many cases.

In the present work, the entrance channel to form the prereactive complex in the OH + CH_2O reaction changes geometry from C_{2v} symmetry (at long distance) to C_s symmetry (at short distance), but the potential energy profile along the minimum-energy path exhibits no local minima or structures of any kind. A bifurcation in the reaction path occurs at the point where the symmetry changes. This produces pronounced variations in the rotational constants and the vibrational frequencies of the normal modes orthogonal to the reaction path, resulting in two reaction flux bottlenecks. Both of these transition states are variational and require a two-TS model based on Miller's unified TST theory. The resulting computed rate constants are in good agreement with the experimental values, and a minor adjustment in barrier height makes the agreement even better. Two-TS models like this one may be required in other reaction systems where a symmetry change occurs along a barrier-less reaction path.

In the OH + CH_2NH reaction system, the dominant reaction under atmospheric conditions is hydrogen abstraction from the N−H bond; at high temperatures, abstraction from the C−H bonds becomes dominant. The pressure dependence is predicted to be relatively weak, except at quite low temperatures. Minor pathways in the OH + CH_2NH reaction system include reactions analogous to these found in the OH + CH_2O and OH + C_2H_4 reaction systems: H abstraction from the CH_2 groups and addition to the sp^2 carbon atom. The relative error in the total rate constants is estimated to be on the order of a factor of ∼2 near 298 K, which reflects the estimated uncertainty of ±0.5 kcal/mol in the computed enthalpies of reaction.

■ ASSOCIATED CONTENT

Supporting Information

Tables of optimized geometries, ro-vibrational parameters, electronic energies, and ZPEs for all of the species involved in the OH + CH_2O, OH + CH_2CH_2, and OH + CH_2NH reactions; tables of electronic energies, ZPE corrections, rate constants, and branching ratios; figures showing rate constants, branching ratios, and internal rotors for the OH + CH_2O, OH + CH_2CH_2, and OH + CH_2NH reactions; and complete refs 30, 31, 41, and 50. This material is available free of charge via the Internet at http://pubs.acs.org.

■ AUTHOR INFORMATION

Notes

The authors declare no competing financial interest.

■ ACKNOWLEDGMENTS

We thank the National Science Foundation (Division of Atmospheric and Geospace Sciences) for financial support. We also thank Jason A. Sonk for useful discussions and preliminary canonical and microcanonical VTST calculations. We are happy to recognize the leadership of Joe Michael, Al Wagner, Larry Harding, and their colleagues at Argonne National Laboratory, who are leaders in combustion science. In particular, J.R.B. gratefully acknowledges his former Ph.D. research advisor, Dr. Joe V. Michael, who was an exceptional teacher-by-example and who continues to show what it means to be a scientist. We also thank the anonymous reviewers for helpful suggestions, including the suggestion to use "GUESS=MIX" when calculating the energies of some transition states.

■ REFERENCES

(1) Onel, L.; Blitz, M.; Dryden, M. B.; Thonger, L.; Seakins, P. Branching Ratios in Reactions of OH Radicals with Methylamine, Dimethylamine, and Ethylamine. *Environ. Sci. Technol.* **2014**, *48*, 9935−9942.

(2) Nielsen, C. J.; Herrmann, H.; Weller, C. Atmospheric Chemistry and Environmental Impact of the Use of Amines in Carbon Capture and Storage (CCS). *Chem. Soc. Rev.* **2012**, *41*, 6684−6704.

(3) Hao, W. M.; Scharffe, D. H.; Lobert, J. M.; Crutzen, P. J. Emissions of Nitrous Oxide from the Burning of Biomass in an Experimental System. *Geophys. Res. Lett.* **1991**, *18*, 999−1002.

(4) Schade, G. W.; Crutzen, P. J. Emission of Aliphatic Amines from Animal Husbandry and Their Reactions: Potential Source of N_2O and HCN. *J. Atmos. Chem.* **1995**, *22*, 319−346.

(5) Rissanen, M. P.; Eskola, A. J.; Nguyen, T. L.; Barker, J. R.; Liu, J.; Liu, J.; Halme, E.; Timonen, R. S. CH_2NH_2 + O_2 and CH_3CHNH_2 + O_2 Reaction Kinetics: Photoionization Mass Spectrometry Experiments and Master Equation Calculations. *J. Phys. Chem. A* **2014**, *118*, 2176−2186.

(6) Quinto-Hernandez, A.; Wodtke, A. M.; Bennett, C. J.; Kim, Y. S.; Kaiser, R. I. On the Interaction of Methyl Azide (CH_3N_3) Ices with Ionizing Radiation: Formation of Methanimine (CH_2NH), Hydrogen Cyanide (HCN), and Hydrogen Isocyanide (HNC). *J. Phys. Chem. A* **2011**, *115*, 250−264.

(7) Pearson, R., Jr.; Lovas, F. J. Microwave Spectrum and Molecular Structure of Methylenimine (CH_2NH). *J. Chem. Phys.* **1977**, *66*, 4149−4156.

(8) Hamada, Y.; Hashiguchi, K.; Tsuboi, M.; Koga, Y.; Kondo, S. Pyrolysis of Amines: Infrared Spectrum of Methyleneimine. *J. Mol. Spectrosc.* **1984**, *105*, 70−80.

(9) Milligan, D. E. Infrared Spectroscopic Study of the Photolysis of Methyl Azide and Methyl-d_3 Azide in Solid Argon and Carbon Dioxide. *J. Chem. Phys.* **1961**, *35*, 1491−1497.

(10) Jacox, M. E.; Milligan, D. E. The Infrared Spectrum of Methylenimine. *J. Mol. Spectrosc.* **1975**, *56*, 333−336.

(11) Teslja, A.; Nizamov, B.; Dagdigian, P. J. The Electronic Spectrum of Methyleneimine. *J. Phys. Chem. A* **2004**, *108*, 4433−4439.

(12) Kaifu, N.; Morimoto, M.; Nagane, K.; Akabane, K.; Iguchi, T.; Takagi, K. Detection of Interstellar Methylamine. *Astrophys. J.* **1974**, *191*, L135−L137.

(13) Godfrey, P. D.; Brown, R. D.; Robinson, B. J.; Sinclair, M. W. Discovery of Interstellar Methanimine (Formaldimine). *Astrophys. Lett.* **1973**, *13*, 119.

(14) Crovisier, J.; Bockelee-Morvan, D.; Colom, P.; Biver, N.; Despois, D.; Lis, D. C. The Composition of Ices in Comet C/1995 O1 (Hale−Bopp) from Radio Spectroscopy—Further Results and Upper Limits on Undetected Species. *Astron. Astrophys.* **2004**, *418*, 1141−1157.

(15) Bernstein, M. P.; Bauschlicher, C. W., Jr.; Sandford, S. A. The Infrared Spectrum of Matrix Isolated Aminoacetonitrile, a Precursor to the Amino Acid Glycine. *Adv. Space Res.* **2004**, *33*, 40−43.

(16) Koch, D. M.; Toubin, C.; Peslherbe, G. H.; Hynes, J. T. A. Theoretical Study of the Formation of the Aminoacetonitrile Precursor of Glycine on Icy Grain Mantles in the Interstellar Medium. *J. Phys. Chem. C* **2008**, *112*, 2972−2980.

(17) Bunkan, A. J. C.; Tang, Y.; Sellevåg, S. R.; Nielsen, C. J. Atmospheric Gas Phase Chemistry of CH_2=NH and HNC. A First-Principles Approach. *J. Phys. Chem. A* **2014**, *118*, 5279−5288.

(18) Georgievskii, Y.; Klippenstein, S. J. Long-Range Transition State Theory. *J. Chem. Phys.* **2005**, *122*, No. 194103.

(19) Glowacki, D. R.; Liang, C.-H.; Morley, C.; Pilling, M. J.; Robertson, S. H. MESMER: An Open-Source Master Equation Solver for Multi-Energy Well Reactions. *J. Phys. Chem. A* **2012**, *116*, 9545−9560.

(20) Barker, J. R. Multiple-Well, Multiple-Path Unimolecular Reaction Systems. I. MultiWell Computer Program Suite. *Int. J. Chem. Kinet.* **2001**, *33*, 232−245.

(21) Barker, J. R. Energy Transfer in Master Equation Simulations: A New Approach. *Int. J. Chem. Kinet.* **2009**, *41*, 748−763.

DOI: 10.1021/acs.jpca.5b00910
J. Phys. Chem. A 2015, 119, 7578−7592

(22) Barker, J. R.; Ortiz, N. F.; Preses, J. M.; Lohr, L. L.; Maranzana, A.; Stimac, P. J.; Nguyen, T. L.; Kumar, T. J. D. Multiwell-2014 Software. http://aoss-research.engin.umich.edu/multiwell/ (accessed Jan 20, 2014).
(23) Atkinson, R. J.; Pitts, J. N. Kinetics of the Reactions of the OH Radical with HCHO and CH_3CHO over the Temperature Range 299−426°K. *J. Chem. Phys.* **1978**, *68*, 3581−3584.
(24) Sivakumaran, V.; Holscher, D.; Dillon, T. J.; Crowley, J. N. Reaction between OH and HCHO: Temperature Dependent Rate Coefficients (202−399 K) and Product Pathways (298 K). *Phys. Chem. Chem. Phys.* **2003**, *5*, 4821−4827.
(25) Vasudevan, V.; Davidson, D. F.; Hanson, R. K. Direct Measurements of the Reaction OH + CH_2O → HCO + H_2O at High Temperatures. *Int. J. Chem. Kinet.* **2005**, *37*, 98−109.
(26) Wang, S.; Davidson, D. F.; Hanson, R. K. High Temperature Measurement for the Rate Constants of C1−C4 Aldehydes with OH in a Shock Tube. *Proc. Combust. Inst.* **2015**, *35*, 473−480.
(27) Xu, S.; Zhu, R. S.; Lin, M. C. Ab Initio Study of the OH + CH_2O Reaction: The Effect of the OH−OCH_2 Complex on the H-Abstraction Kinetics. *Int. J. Chem. Kinet.* **2006**, *38*, 322−326.
(28) Zhang, W.; Du, B.; Qin, Z. Catalytic Effect of Water, Formic Acid, or Sulfuric Acid on the Reaction of Formaldehyde with OH Radicals. *J. Phys. Chem. A* **2014**, *118*, 4797−4807.
(29) Atkinson, R.; Baulch, D. L.; Cox, R. A.; Hampson, R. F.; Kerr, J. A.; Rossi, M. J.; Troe, J. Evaluated Kinetic and Photochemical Data for Atmospheric Chemistry, Organic Species: Supplement VII IUPAC Subcommittee on Gas Kinetic Data Evaluation for Atmospheric Chemistry. *J. Phys. Chem. Ref. Data* **1999**, *28*, 191−390.
(30) Baulch, D. L.; Bowman, C. T.; Cobos, C. J.; et al. Evaluated Kinetics Data for Combustion Modeling: Supplement II. *J. Phys. Chem. Ref. Data* **2005**, *34*, 757−1397.
(31) Sander, S. P.; Friedl, R. R.; Barker, J. R.; et al. *Chemical Kinetics and Photochemical Data for Use in Atmospheric Studies: Evaluation Number 17*; JPL Publication 10-6; Jet Propulsion Laboratory: Pasadena, CA, 2011.
(32) Vakhtin, A. B.; Murphy, J. E.; Leone, S. R. Low-Temperature Kinetics of Reactions of OH Radical with Ethene, Propene, and 1-Butene. *J. Phys. Chem. A* **2003**, *107*, 10055−10062.
(33) Tully, F. P. Hydrogen-Atom Abstraction from Alkenes by OH. Ethylene and 1-Butene. *Chem. Phys. Lett.* **1988**, *143*, 510−514.
(34) Atkinson, R. Gas-Phase Tropospheric Chemistry of Volatile Organic Compounds: 1. Alkanes and Alkenes. *J. Phys. Chem. Ref. Data* **1997**, *26*, 215−290.
(35) DeMore, W. B.; Sander, S. P.; Golden, D. M.; Hampson, R. F.; Kurylo, M. J.; Howard, C. J.; Ravishankara, A. R.; Kolb, C. E.; Molina, M. J. *Chemical Kinetics and Photochemical Data for Use in Stratospheric Modeling: Evaluation Number 12*; JPL Publication 97-4; Jet Propulsion Laboratory: Pasadena, CA, 1997.
(36) Golden, D. M. The Reaction OH + C_2H_4: An Example of Rotational Channel Switching. *J. Phys. Chem. A* **2012**, *116*, 4259−4266.
(37) Greenwald, E. E.; North, S. W.; Georgievskii, Y.; Klippenstein, S. J. A Two Transition State Model for Radical−Molecule Reaction: A Case Study of the Addition of OH to C_2H_4. *J. Phys. Chem. A* **2005**, *109*, 6031−6044.
(38) Senosiain, J. P.; Klippenstein, S. J.; Miller, J. A. Reaction of Ethylene with Hydroxyl Radicals: A Theoretical Study. *J. Phys. Chem. A* **2006**, *110*, 6960−6970.
(39) Cleary, P. A.; Romero, M. T. B.; Blitz, M. A.; Heard, D. E.; Pilling, M. J.; Seakins, P. W.; Wang, L. Determination of the Temperature and Pressure Dependence of the Reaction OH + C_2H_4 from 200−400 K using Experimental and Master Equation Analyses. *Phys. Chem. Chem. Phys.* **2006**, *8*, 5633−5642.
(40) Zhu, R. S.; Park, J.; Lin, M. C. Ab Initio Kinetic Study on the Low-Energy Paths of the HO + C_2H_4 Reaction. *Chem. Phys. Lett.* **2005**, *408*, 25−30.
(41) Frisch, M. J.; Trucks, G. W.; Schlegel, H. B.; et al. *Gaussian 09*, revision C.01; Gaussian Inc.: Wallingford, CT, 2013.
(42) Becke, A. D. A New Mixing of Hartree−Fock and Local Density-Functional Theories. *J. Chem. Phys.* **1993**, *98*, 1372−1377.
(43) Kendall, R. A.; Dunning, T. H., Jr.; Harrison, R. Electron Affinities of the First Row Atoms Revisited. Systematic Basis Sets and Wave Functions. *J. Chem. Phys.* **1992**, *96*, 6796−6806.
(44) Woon, D. E.; Dunning, T. H., Jr. Gaussian Basis Sets for Use in Correlated Molecular Calculations. III. The Atoms Aluminum Through Argon. *J. Chem. Phys.* **1993**, *98*, 1358−1371.
(45) Becke, A. D. Density-Functional Thermochemistry. III. The Role of Exact Exchange. *J. Chem. Phys.* **1993**, *98*, 5648−5652.
(46) Raghavachari, K.; Trucks, G. W.; Pople, J. A.; Head-Gordon, M. A Fifth-Order Perturbation Comparison of Electron Correlation Theories. *Chem. Phys. Lett.* **1989**, *157*, 479−483.
(47) Nguyen, H. M. T.; Nguyen, H. T.; Nguyen, T.-N.; Hoang, H. V.; Vereecken, L. Theoretical Study on the Reaction of the Methylidyne Radical, $CH(X^2\Pi)$, with Formadehyde, CH_2O. *J. Phys. Chem. A* **2014**, *118*, 8861−8871.
(48) Li, S.; Dames, S. E.; Davidson, D. F.; Hanson, R. K. High-Temperature Measurement of the Reaction of OH with Ethylamine and Dimethylamine. *J. Phys. Chem. A* **2014**, *118*, 70−77.
(49) Bråten, H. B.; Bunkan, A. J.; Bache-Andreassen, L.; Solimannejad, M.; Nielsen, C. J. *Final Report on a Theoretical Study on the Atmospheric Degradation of Selected Amines*; University of Oslo: Oslo, Norway, 2009.
(50) Stanton, J. F.; Gauss, J.; Harding, M. E.; et al. *CFOUR: A Quantum Chemical Program Package*, version 1.2; University of Texas: Austin, TX, 2010.
(51) Klippenstein, S. J.; Pande, V. S.; Truhlar, D. G. Chemical Kinetics and Mechanism of Complex Systems: A Perspective on Recent Theoretical Advances. *J. Am. Chem. Soc.* **2014**, *136*, 528−546.
(52) Barker, J. R.; Nguyen, T. L.; Stanton, J. F. Kinetic Isotope Effects for Cl + CH_4 ⇄ HCl + CH_3 Calculated Using Ab Initio Semiclassical Transition State Theory. *J. Phys. Chem. A* **2012**, *116*, 6408−6419.
(53) Nguyen, T. L.; Xue, B. C.; Weston, R. E., Jr.; Barker, J. R.; Stanton, J. F. Reaction of HO with CO: Tunneling Is Indeed Important. *J. Phys. Chem. Lett.* **2012**, *3*, 1549−1553.
(54) Jasper, A. W.; Klippenstein, S. J.; Harding, L. B. The Effect of Spin−Orbit Splitting on the Association Kinetics of Barrierless Atom−Hydrocarbon Radical Reactions. *J. Phys. Chem. A* **2010**, *114*, 5759−5768.
(55) Fukui, K. The Path of Chemical Reactions—The IRC Approach. *Acc. Chem. Res.* **1981**, *14*, 363−375.
(56) Hratchian, H. P.; Schlegel, H. B. In *Theory and Applications of Computational Chemistry: The First Forty Years*; Dykstra, C. E., Frenking, G., Kim, K. S., Scuseria, G. E., Eds.; Elsevier: Amsterdam, 2005; Chapter 10.
(57) Rienstra-Kiracofe, J. C.; Allen, W. D.; Schaefer, H. F., III. The C_2H_5 + O_2 Reaction Mechanism: High-Level Ab Initio Characterizations. *J. Phys. Chem. A* **2000**, *104*, 9823−9840.
(58) Forst, W. *Unimolecular Reactions: A Concise Introduction*; Cambridge University Press: Cambridge, U.K., 2003.
(59) Coxon, J. A.; Foster, S. C. Radical Dependence of Spin Orbit and Lambda-Doubling Parameters in the $X^2\Pi$ Ground-State of Hydroxyl. *J. Mol. Spectrosc.* **1982**, *91*, 243−254.
(60) Nielsen, A.; Holder, A. *GaussView 3.0 User's Reference*; Gaussian, Inc.: Pittsburgh, PA, 2003.
(61) Bafiares, L.; Alonso, J.; Menzinger, M.; Urefia, A. G. Microcanonical Variational Transition State Theory: Quasi-Collinear Configurations Application to the Cl + CH_3I → ClI + CH_3 Excitation Function. *J. Chem. Soc., Faraday Trans.* **1986**, *82*, 1033−1041.
(62) Truhlar, D. G.; Garrett, B. C. Variational Transition State Theory. *Annu. Rev. Phys. Chem.* **1984**, *35*, 159−189.
(63) Truhlar, D. G.; Garrett, B. C. Generalized Transition State Theory. Classical Mechanical Theory and Applications to Collinear Reactions of Hydrogen Molecules. *J. Phys. Chem.* **1979**, *83*, 1052−1078.

DOI: 10.1021/acs.jpca.5b00910
J. Phys. Chem. A 2015, 119, 7578−7592

(64) Baboul, A. G.; Schlegel, H. B. Improved Method for Calculating Projected Frequencies along a Reaction Path. *J. Chem. Phys.* **1997**, *107*, 9413−9417.
(65) Ali, M. A.; Dillstrom, V. T.; Lai, J. Y. W.; Violi, A. Ab Initio Investigation of the Thermal Decomposition of *n*-Butylcyclohexane. *J. Phys. Chem. A* **2014**, *118*, 1067−1076.
(66) Ali, M. A.; Violi, A. Reaction Pathways for the Thermal Decomposition of Methyl Butanoate. *J. Org. Chem.* **2013**, *78*, 5898−5908.
(67) Stein, S. E.; Rabinovitch, B. S. Accurate Evaluation of Internal Energy Level Sums and Densities Including Anharmonic Oscillators and Hindered Rotors. *J. Chem. Phys.* **1973**, *58*, 2438−2445.
(68) Beyer, T.; Swinehart, D. F. Number of Multiply-Restricted Partitions. *Commun. ACM* **1973**, *16*, 379−379.
(69) Goldsmith, C. F.; Green, W. H.; Klippenstein, S. J. Role of O_2 + QOOH in Low-Temperature Ignition of Propane. 1. Temperature and Pressure Dependent Rate Coefficients. *J. Phys. Chem. A* **2012**, *116*, 3325−3346.
(70) Hippler, J.; Troe, J.; Wendelken, H. J. Collisional Deactivation of Vibrationally Highly Excited Polyatomic Molecules. II. Direct Observations for Excited Toluene. *J. Chem. Phys.* **1983**, *78*, 6709−6717.
(71) Ruscic, B. Thermochemical Tables (ATcT) values based on ver. 1.112 of the Thermochemical Network, 2013.
(72) Miller, W. H. Unified Statistical Model for "Complex" and "Direct" Reaction Mechanisms. *J. Chem. Phys.* **1976**, *65*, 2216−2223.

DOI: 10.1021/acs.jpca.5b00910
J. Phys. Chem. A 2015, 119, 7578−7592